

Forming of Multilayer Sheet Metal by Drawing Process: An Analysis and FEM Simulation

Y. Mollapour^{1*}, D. Afshari² and H. Haghghat³

^{1,2}Department of Mechanical Engineering, University of Zanjan, Zanjan, Iran.

³Department of Mechanical Engineering, Razi University, Kermanshah, Iran.

Abstract: In this paper, the drawing process of multilayer sheet metal through a wedge-shaped die has been analyzed using stream function and upper bound method. Typically, a sandwich sheet contains three layers of metal, where the outer layers are of the same thickness and material and different from those of the inner layer. In this study, a new deformation model has been introduced in which inlet and outlet shear boundaries are considered flexible and the effect of work hardening of sheet layer materials has been considered. According to the suggested stream function, velocity field, strain rates and powers have been calculated. The optimized geometry of the deformation zone and the required drawing force have been determined depending on the process conditions. Analytical results including the drawing force and thickness of the sheets in the outlet of the die have been compared with the finite element (FE) results. The FE results have good congruence with the analytical ones. Finally, the effects of friction factor and reduction in thickness have been investigated on the drawing force and the optimum die angle.

Keywords: Upper bound, Work hardening, Sheet Drawing, Deformation zone, Stream function.

1. Introduction

Multilayer materials are widely developed in various industries because homogeneous monolayer materials cannot have all of the requirements. Combination of different layers to reach various properties is highly demanded in many industries such as automotive, aviation and electrical industries, power plants, oil, gas, petrochemical, containers and pressure vessels. The sandwich sheets are composed of two or more metals bonded to each other, and their manufacturing using metal forming processes is an important issue. Drawing processes including forming processes are used to fuse and reduce the thickness of multilayer sheet metals. Stretching, cold welding and metallurgical bonds between the layers occur in the drawing process due to the compressive stresses produced by passing the sheets from the die. As a result, this process is one of the most widely used processes to manufacture multi-layer sheet metals.

In this process, such as other metal forming processes, predicting of the forming force and the attempt to minimize it are very important. Estimating the force required to forming the sheets is the key factor to design and select the die and tools. In addition to that, reducing the forming force has multiple benefits such as reducing the energy consumption and increasing the life of the die.

Some researchers have used the upper bound method and FE model to analyze multilayer sheet metal drawing process. Multimetal sheet process was tested and analyzed for the first time by Arnold Van [1] in 1958 using the cold rolling process. Atkins and Weinstein [2] investigated the deformation of sandwich sheets under different processes including simple tension, tension, extrusion from inside the die, plane strain compression, and rolling. They considered these processes as a plane strain problem, and investigated the value of tensile or compressive stresses based on force balance equations. Both sliding

friction and constant shear stress were considered separately to model the friction between the work pieces and the die.

Osakada and Niimi [3] analyzed axially symmetric extrusion in a conical die. They used the upper bound method to analyze this process. They suggested applying the generalized term to radial flow field and assuming it as the same for both input and output boundary deformation zones. In a special case, their proposed boundary was the spherical boundary presented by Avitzur [4]. In 1984, David Durban [5] investigated the drawing and extrusion in sheets, wires, and multimetal tubes in conical dies. His assumptions included the full rigid-plastic processes and the plane strain sheets. Durban used the method proposed by Nadai-Hill for the radial flow field plane strain and the shield method for the three-dimensional radial flow. Tokuno [6] tested and analyzed the mono and multilayer rods extrusion with the upper bound method. Experimental results showed that the material stream lines within the deformation zone were not only straight but also curvature. Taheri and Majlesi [7], studied the drawing process of the bimetal and three-metal sheets through the wedge-shaped die. They studied various and different die angles and measured the tensile stress. They indicated that manufacturing by this method is possible, although the interlayer strength is very low for a thickness reduction of less than 8%. Taheri [8] also studied and analyzed the upper bound of multilayer sheet metals drawing and compared its results with experimental results. In this study the inner and outer boundaries were considered as two straight and parallel lines that were perpendicular to the drawing axis. Chitkara and Aleem [9, 10] theoretically studied the mechanics of the extrusion of axisymmetric bimetallic tubes from solid circular billets using fixed mandrel with the application of generalized upper bound and slab method analyses. They investigated the effect of different parameters such as extrusion ratio, frictional conditions, and the shape of the dies and that of the mandrels on the extrusion pressures. Hwang and Hwang [11] studied the plastic deformation behavior within a conical die during composite rod extrusion by experimental and upper bound methods. They showed that the results of the presented analysis and the experimental test are close to each other. Rubio et al [12] analyzed the drawing sheet under conditions of plane strain upper bound method in a wedge-shaped die. Their idea in this paper was to divide the deformation area into a number of triangular rigid blocks with linear input and output boundaries. In this research, they investigated the effect of the number of blocks on calculating the tension in the sheets. Kazanowski et al. [13] discussed the influence of initial bimaterial billet geometry on the dimensions of the final product. The flat face die was used for all experiments and the proposed bimaterial billet design modifications were evaluated experimentally and by finite element modeling. Nowotynska and Smykla [14] studied the influence of the geometric parameters of the die on the plastic flow of layer composites during extrusion process by the experimental method. Khosravifard and Ebrahimi [15] analyzed the extrusion of Al/Cu bimetal rod through conical dies by FEM and studied the effect of the extrusion parameters on the creation of interfacial bonds. Maleki et al [16], analyzed the upper bound stretch of the thin bimetal sheet and compared it with the experimental tests. In their study, the deformation zone was divided into rigid zones. The relative velocity between every pair of the rigid zones was calculated on discontinuities surfaces to estimate shear power losses. Haghghat and Amjadian [17] and Haghghat and Shayesteh [18] investigated the bimetal sheets extrusion process by the upper bound method and FE simulation. Panteghini [19] analyzed the process of drawing sheet using the upper bound method and slab method. The die shape was designed in order to reduce the thickness and width of the sheet at the same time. He solved the upper bound considering the deformation zone as tetragonal rigid blocks and linear boundaries.

Literature review indicates that the deformation zone boundaries in the forming process are not fixed and they vary depending on the process conditions. In this paper, an analytical deformation model has been developed by assuming that inlet and outlet shear boundaries are flexible. In addition, the effect of work hardening of sheet layer materials has been considered in the presented model. Sheet layers are

separated before the process and they bind with each other after leaving the die. Considering the inlet and outlet as flexible boundaries and applying the work hardening to the analytical analysis leads to good congruence between the results obtained from the analytical and FE model.

2. Mathematical Model

Throughout the analyses, the following assumptions are employed:

- 1- The deformation in the sheet is plane strain.
- 2- The die is rigid.
- 3- The material is homogeneous and incompressible, and it follows of von Mises flow law.

Figure 1 illustrates the schematic of the drawing process of multi-layer sheet metal through a wedge-shaped die. The sheet has three layers. Although the thickness and material type of the outer layers are the same, they are different from the inner layer.

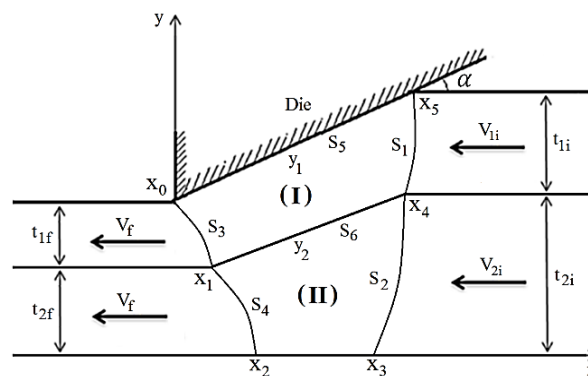


Fig. 1. Symmetrical multilayer sheet metal drawing process, geometric parameters and deformation zones.

As Fig. 1 presents, the sheet with t_{1i} , V_{1i} (thickness and velocity of the outer layer) and t_{2i} , V_{2i} (thickness and velocity of the inner layer) enter the wedge-shaped die with a semi angle α . Before the process the inner and outer layers are separated, and they stick together when they leave the die. t_{1f} , t_{2f} and V_{1f} , V_{2f} represent the thickness of the outer layer, the inner layer and the velocity of the multilayer sheet when it leaves the die. The plastic deformation zone is divided into two zones, which are shown in Fig. 1 by zone I and zone II. Zones I and II are the relevant outer and inner layers, respectively.

2.1. Stream functions

The flow pattern of the plastic deformation in each zone is assumed to be represented by a single stream function denoted by ϕ_1 and ϕ_2 , respectively, as follows:

$$\begin{aligned}\phi_1 &= Q_1[\eta + C_1(y - y_2)(y - y_1)] \\ \phi_2 &= Q_2\left[\frac{y}{y_2} + C_2y(y - y_2)\right]\end{aligned}\quad (1)$$

$$\begin{aligned}y_1 &= y_1(x) = t_f + \frac{t_1 - t_f}{L_{1i}}x \\ y_2 &= y_2(x) = t_{2f} + \frac{t_{2i} - t_{2f}}{L_{2i} - L_{2f}}x \\ \eta &= \frac{y - y_2}{y_1 - y_2}\end{aligned}\quad (2)$$

where Q_1 and Q_2 represent the volume flow rate at each cross-section of zones I and II. y_1 and y_2 are boundary functions along the die surface and the interface between the sheets, respectively. y_2 function is assumed to be linear, and its slope may differ from that of y_1 . The stream function mentioned in Eq. (1) is composed of two parts. The first part shows a steady stream along the perpendicular cross section in the

die, while the second part represents a non-uniform flow perpendicular to the cross section with a flow rate of zero. C_1 and C_2 values are assumed to be quadratic functions of x :

$$C_1 = a_1 x^2 + b_1 \quad (3)$$

$$C_2 = a_2 x^2 + b_2 \quad (4)$$

where a_1 , b_1 , a_2 and b_2 are constant and determined by boundary conditions.

2.2. Velocity fields

The velocity field that is used for plane strain analysis of the flow in a wedge-shaped die is in the Cartesian coordinate system. In this process, the horizontal and vertical components of the velocity are extracted directly from the streams ϕ_1 and ϕ_2 , and z component of the velocity is zero because the process is plane strain. For the upper bound analysis, when the deformation zone is divided into smaller zones, the velocity fields in each zone should be specified. The velocity field must satisfy the boundary conditions and the incompressibility condition.

The full velocity field for the flow of the material in the deformation zone is obtained by invoking volume constancy. The volume constancy in Cartesian coordinate system is defined as:

$$\dot{\epsilon}_{ii} = \dot{\epsilon}_{xx} + \dot{\epsilon}_{yy} + \dot{\epsilon}_{zz} = 0 \quad (5)$$

The velocity fields in each zone are calculated from Eqs. (6)-(9). The horizontal and vertical velocities in the outer layer V_x and V_y can be derived directly from the stream function ϕ .

2.2.1. Zone (I)

The velocity field in this zone is calculated from Eq. (6):

$$V_x = \frac{\partial \phi_1}{\partial y} = Q_1 \left[\frac{1}{y_1 - y_2} + 2C_1 \left\{ y - \frac{y_1 + y_2}{2} \right\} \right]$$

$$V_y = -\frac{\partial \phi_1}{\partial x} = -Q_1 [\eta' + C_1'(y - y_1)(y - y_2) - C_1(y - y_2)y_1' - C_1(y - y_1)y_2'] \quad (6)$$

$$\eta' = \frac{(y_1 - y_2)(-y_2') - (y - y_2)(y_1' - y_2')}{(y_1 - y_2)^2}$$

where $(\dot{})$ denotes the derivative of () with respect to x .

By substituting $y = y_1$ in Eq. (6):

$$\left[\frac{V_y}{V_x} \right]_{y=y_1} = \frac{y_1'/(y_1 - y_2) + C_1 y_1'(y_1 - y_2)}{1/(y_1 - y_2) + C_1(y_1 - y_2)} = y_1' \quad (7)$$

and by substituting $y = y_2$ in Eq. (6), similarly:

$$\left[\frac{V_y}{V_x} \right]_{y=y_2} = y_2' \quad (8)$$

Equations. (7) and (8) show that the equation obtained from Eq. (1), satisfies the boundary conditions along the die surface and between two metal surfaces.

2.2.2. Zone (II)

The velocity field in this zone is calculated from Eq. (9):

$$V_x = \frac{\partial \phi_2}{\partial y} = Q_2 \left[\frac{1}{y_2} + 2C_2 \left(y - \frac{y_2}{2} \right) \right]$$

$$V_y = -\frac{\partial \phi_2}{\partial x} = -Q_2 y \left[\frac{-y_2'}{y_2^2} + C_2'(y - y_2) - C_2 y_2' \right] \quad (9)$$

Like zone (I), the velocity boundary conditions are also met for this area.

2.3. Incompressibility condition

The strain rates in a Cartesian coordinate system are defined as:

$$\begin{aligned}\dot{\epsilon}_{xx} &= \frac{\partial V_x}{\partial x} \\ \dot{\epsilon}_{yy} &= \frac{\partial V_y}{\partial y} \\ \dot{\epsilon}_{zz} &= \frac{\partial V_z}{\partial z}\end{aligned}\tag{10}$$

$$\dot{\epsilon}_{xy} = \frac{1}{2} \left(\frac{\partial V_x}{\partial y} + \frac{\partial V_y}{\partial x} \right)$$

and the normal strain rates component is defined as:

$$\begin{aligned}\dot{\epsilon}_{xx} &= \frac{\partial V_x}{\partial x} = \frac{\partial^2 \phi}{\partial y \partial x} \\ \dot{\epsilon}_{yy} &= \frac{\partial V_y}{\partial y} = -\frac{\partial^2 \phi}{\partial x \partial y} \\ \dot{\epsilon}_{zz} &= \frac{\partial V_z}{\partial z} = 0\end{aligned}\tag{11}$$

$$+\dot{\epsilon}_{yy} + \dot{\epsilon}_{zz} = 0\dot{\epsilon}_{xx}$$

Equation (11) shows that the sum of the normal strain rate is zero, so all the arbitrary stream function satisfies the incompressibility condition.

2.4. Boundary function of the deformation zones

The sheet has a uniform velocity before it flows in the die and also after it leaves the die. The boundary conditions for the flow function, resulting from the boundary conditions for velocity and flow function continuity, are as follows:

$$\phi_{1i} = Q_1 \left(\frac{y - t_{2i}}{t_{1i}} \right) \quad \text{On } S_1 \text{ boundary} \tag{12}$$

$$\phi_{2i} = Q_2 \left(\frac{y}{t_{2i}} \right) \quad \text{On } S_2 \text{ boundary} \tag{13}$$

$$\phi_{1f} = Q_1 \left(\frac{y - t_{2f}}{t_{1f} - t_{2f}} \right) \quad \text{On } S_3 \text{ boundary} \tag{14}$$

$$\phi_{2f} = Q_2 \left(\frac{y}{t_{2f}} \right) \quad \text{On } S_4 \text{ boundary} \tag{15}$$

By applying the continuity of the flow lines ($\phi_1 = \phi_{1i}$) to the inlet of the die, y_{S1} can be calculated using the following equation:

$$y_{S1} = \begin{cases} \frac{-B_1 + \sqrt{B_1^2 - 4A_1C_1}}{2C_1}; & x_4 < x_5 \\ \frac{-B_1 - \sqrt{B_1^2 - 4A_1C_1}}{2C_1}; & x_4 > x_5 \end{cases}, \tag{16}$$

$$B_1 = \frac{1}{y_1 - y_2} - C_1(y_1 + y_2) - \frac{1}{t_{1i}},$$

$$A_1 = C_1 y_1 y_2 - \frac{y_2}{y_1 - y_2} + \frac{t_{2i}}{t_{1i}}$$

For the inlet boundary of the inner sheet, from $\phi_2 = \phi_{2i}$ in the inlet of the die, the boundary function S_2 is

$$y_{S2} = y_2 + \frac{1/t_{2i} - 1/y_2}{C_2} \quad (17)$$

The material velocity is steady after the material leaves the die. As a result, boundary functions y_{S3} and y_{S4} for the inlet and outlet layers respectively can be calculated using the following equation:

$$y_{S3} = \frac{-B_2 - \sqrt{B_2^2 - 4A_2C_1}}{2C_1},$$

$$B_2 = \frac{1}{y_1 - y_2} - C_1(y_1 + y_2) - \frac{1}{t_{1f}} \quad (18)$$

$$A_2 = C_1 y_1 y_2 - \frac{y_2}{y_1 - y_2} + \frac{t_{2f}}{t_{1f}}$$

$$y_{S4} = y_2 + \frac{1/t_{2f} - 1/y_2}{C_2} \quad (19)$$

2.5. Boundary conditions

From the geometrical boundary condition $y_{s1}(x_4) = t_{2i}$ and $y_{s3}(x_1) = t_{2f}$, constants a_1 and b_1 in Eqs. (3) and (4) can be calculated using the following equation:

$$a_1 = \frac{1}{x_4 - x_1} (I_{1i} - I_{1f})$$

$$b_1 = I_{1i} - a_1 x_4^2$$

$$I_{1i} = \frac{1}{y_1(x_4)} \left(\frac{1}{y_1(x_4)} - \frac{1}{t_{1i} + t_{2i}} \right) \quad (20)$$

$$I_{1f} = \frac{1}{y_1(x_1)} \left(\frac{1}{y_1(x_1)} - \frac{1}{t_{1f} + t_{2f}} \right)$$

From geometrical boundary condition $y_{s2}(x_3) = 0$ and $y_{s4}(x_2) = 0$, constants a_2 and b_2 in Eqs. (3) and (4) can be calculated using the following equation:

$$a_2 = \frac{1}{x_3 - x_2} (I_{2i} - I_{2f})$$

$$b_2 = I_{2i} - a_2 x_3^2$$

$$I_{2i} = \frac{1}{y_2(x_3)} \left(\frac{1}{y_2(x_3)} - \frac{1}{t_{2i}} \right) \quad (21)$$

$$I_{2f} = \frac{1}{y_2(x_2)} \left(\frac{1}{y_2(x_2)} - \frac{1}{t_{2f}} \right)$$

2.6. Strain rate components

By calculating the velocity field in different deformation zones, the strain rate in each zone can be calculated by the velocity field of the related zone and Eq. (6).

2.6.1. Zone (I)

The strain rate in zone (I) is determined by Eq. (22):

$$\begin{aligned}\dot{\varepsilon}_{xx} &= Q_1 \left[\frac{y_2' - y_1'}{(y_1 - y_2)^2} - C_1'(y_1 + y_2 - 2y) - C_1(y_1' + y_2') \right] \\ \dot{\varepsilon}_{yy} &= -Q_1 \left[\frac{y_2' - y_1'}{(y_1 - y_2)^2} - C_1'(y_1 + y_2 - 2y) - C_1(y_1' + y_2') \right] \\ \dot{\varepsilon}_{xy} &= \frac{1}{2} Q_1 [+2C_1 - \eta'' - C_1''(y - y_1)(y - y_2) + 2C_1'(y - y_2)y_1' + 2C_1'(y - y_1)y_2' - 2C_1y_1'y_2']\end{aligned}\quad (22)$$

2.6.2. Zone (II)

The strain rate in zone (II) is determined by Eq. (23):

$$\begin{aligned}\dot{\varepsilon}_{xx} &= Q_2 \left[\frac{y_2'}{y_2^2} + 2C_2'(y - \frac{y_2}{2}) - C_2y_2' \right] \\ \dot{\varepsilon}_{yy} &= -Q_2 \left[\frac{y_2'}{y_2^2} + 2C_2'(y - \frac{y_2}{2}) - C_2y_2' \right] \\ \dot{\varepsilon}_{xy} &= \frac{1}{2} Q_2 \left[2C_2 - 2\frac{yy_2'^2}{y_2^3} - C_2''y(y - y_2) + 2C_2'yy_2' \right]\end{aligned}\quad (23)$$

2.7. Powers

The total power required for the forming process can be divided into three types:

- 1- Internal power of deformation
- 2- Shear power losses
- 3- Friction power losses

Therefore, according to Fig. 1, the total power is the sum of the internal power of deformation, shear power losses and friction power losses.

2.7.1. Internal power of deformation

The internal power of deformation in the upper bound model is:

$$\dot{W}_i = \int_S \bar{\sigma} \dot{\varepsilon}_{eq} dv \quad (24)$$

The internal powers of the inlet and outlet zones are zero. Since the strain rate components in these zones are zero and the material moves rigidly in these zones, no deformation occurs. is the volume element in dv the deformation zone and according to the plane strain process ($t = 1$) is calculated as:

$$= t dx dy = dx dy \quad dv \quad (25)$$

Effective strain rate in the plastic zone is determined by:

$$\dot{\varepsilon}_{eq} = \sqrt{\frac{2}{3} (\dot{\varepsilon}_{xx}^2 + \dot{\varepsilon}_{yy}^2 + 2\dot{\varepsilon}_{xy}^2)} \quad (26)$$

In Eq. (24), $\bar{\sigma}$ is the flow stress of the material and determined by:

$$\bar{\sigma} = A(\bar{\varepsilon})^n \text{MPa} \quad (27)$$

Where A and n are the strength factor and the work hardening exponent respectively and can be obtained from the tensile test for different materials. $\bar{\varepsilon}$ is the effective strain along the stream line and determined by:

$$\bar{\epsilon} = \int_S d\epsilon_{eq} = \int_S \frac{d\epsilon_{eq}}{dt} \frac{dt}{dS} dS = \int_S \frac{\dot{\epsilon}_{eq}}{\sqrt{V_x^2 + V_y^2}} dS \quad (28)$$

In Eq. (28), S is the length of the line particle displacement from the inlet boundary to the outlet boundary. The material flow lines can be drawn using the velocity field (Eqs. (14) and (15)) if this material flow assumes the behavior of the fluid moving by the velocity field.

According to the Euler express, the particles are fixed for the observer in coordinates (x,y) and they don't move with the material. For each point of the deformation zone, the material velocity in two-dimensions, is followed by Eq. (29).

$$Q = [\dot{U}_x(x,y), \dot{U}_y(x,y)] \quad (29)$$

An equation is needed to track the route of each particle and find its position. This equation is based on the velocity and the time which is determined by Eq. (23):

$$Q = [x'(t), y'(t)] \quad (30)$$

Therefore, according to Eqs. (29) and (30) it is as follows:

$$\begin{aligned} \frac{dx}{dt} &= \dot{U}_x(x,y) \\ \frac{dy}{dt} &= \dot{U}_y(x,y) \end{aligned} \quad (31)$$

It is assumed that at $t=0$, the particle is in point (x_1, y_1) on boundary y_{si} to use the numerical solution and the Euler method in order to find the movement distance of each particle in the deformation zone, (Fig. 2). The velocity field in that point is $Q = [\dot{U}_x(x_1, y_1), \dot{U}_y(x_1, y_1)]$. After a while (Δt) , the particle moves to point (x_2, y_2) . As a result:

$$(x_2, y_2) = (x_1 + \Delta t \dot{U}_x(x_1, y_1), y_1 + \Delta t \dot{U}_y(x_1, y_1)) \quad (32)$$

This method is repeated until the line particle arrives to boundary y_{af} . Therefore:

$$(x_{n+1}, y_{n+1}) = (x_n + \Delta t \dot{U}_x(x_n, y_n), y_n + \Delta t \dot{U}_y(x_n, y_n)) \quad (33)$$

Finally, the particle displacement line (S) will be determined by connecting of all the points. Therefore, other flow lines can be determined by repeating this method for another points on boundaries in Eq. (27), the internal power of zones $\bar{\epsilon}$ is determined by Eq. (28) and replacing $\bar{\epsilon}$. Therefore, y_{s2} and y_{s1} I and II is calculated.

$$W_{i1} = \begin{cases} \int_0^{x_1} \int_{y_{s3}}^{y_1} \sigma_s \dot{\epsilon} dy dx + \int_{x_1}^{x_4} \int_{y_2}^{y_1} \sigma_s \dot{\epsilon} dy dx \\ \quad + \int_{x_4}^{x_5} \int_{y_{s1}}^{y_1} \sigma_s \dot{\epsilon} dy dx; \quad x_4 < x_5 \\ \int_0^{x_1} \int_{y_{s3}}^{y_1} \sigma_s \dot{\epsilon} dy dx + \int_{x_1}^{x_5} \int_{y_2}^{y_1} \sigma_s \dot{\epsilon} dy dx \\ \quad + \int_{x_5}^{x_4} \int_{y_2}^{y_{s1}} \sigma_s \dot{\epsilon} dy dx; \quad x_4 > x_5 \end{cases} \quad (34)$$

$$W_{i2} = \begin{cases} \int_{x_1}^{x_2} \int_{y_{s4}}^{y_2} \sigma_c \dot{\epsilon} dy dx + \int_{x_2}^{x_3} \int_0^{y_2} \sigma_c \dot{\epsilon} dy dx \\ \quad + \int_{x_3}^{x_4} \int_{y_{s2}}^{y_2} \sigma_c \dot{\epsilon} dy dx; \quad x_3 < x_4 \\ \int_{x_1}^{x_2} \int_{y_{s4}}^{y_2} \sigma_c \dot{\epsilon} dy dx + \int_{x_2}^{x_4} \int_0^{y_2} \sigma_c \dot{\epsilon} dy dx \\ \quad + \int_{x_4}^{x_3} \int_0^{y_{s2}} \sigma_c \dot{\epsilon} dy dx; \quad x_3 > x_4 \end{cases}$$

And the total internal power is:

$$W_i = W_{i1} + W_{i2} \quad (35)$$

2.7.2. Shear power losses

The equation for the power losses along the shear surface of the velocity discontinuity is:

$$W_s = \frac{1}{\sqrt{3}} \int_S \sigma |\Delta V| dS \quad (36)$$

There are four different velocity discontinuity surfaces in multilayer sheet metal drawing process that are defined by Eqs. (37)-(39).

For the velocity discontinuity surface S_1 :

$$\Delta V_1 = \begin{cases} V_y \frac{dy}{dS} + (V_x - V_{1i}) \frac{dx}{dS}; & x_4 < x_5 \\ V_y \frac{dy}{dS} - (V_x + V_{1i}) \frac{dx}{dS}; & x_4 > x_5 \end{cases} \quad (37)$$

For surface S_2 :

$$\Delta V_2 = \begin{cases} V_y \frac{dy}{dS} + (V_x - V_{2i}) \frac{dx}{dS}; & x_3 < x_4 \\ V_y \frac{dy}{dS} - (V_x + V_{2i}) \frac{dx}{dS}; & x_3 > x_4 \end{cases} \quad (38)$$

For surfaces S_3 and S_4 :

$$\Delta V_3 = \Delta V_4 = \begin{cases} V_y \frac{dy}{dS} - (V_x + V_f) \frac{dx}{dS}; & x_0 < x_1, x_1 < x_2 \\ V_y \frac{dy}{dS} + (V_x - V_f) \frac{dx}{dS}; & x_0 > x_1, x_1 > x_2 \end{cases} \quad (39)$$

The equal strain of the velocity discontinuity surfaces is determined by Eq. (40):

$$\epsilon_s = \frac{\gamma_s}{\sqrt{3}} \quad (40)$$

Where γ_s is the engineering shear strain on the velocity discontinuity surface and is given in Eqs. (41)-(44):

$$\gamma_{s1} = \frac{|\Delta V_1|}{|U_1|} = \frac{|\Delta V_1|}{\sqrt{[V_i - V_x(x, y_{s1})]^2 + V_y^2(x, y_{s1})}} \quad (41)$$

$$\gamma_{s2} = \frac{|\Delta V_2|}{|U_2|} = \frac{|\Delta V_2|}{\sqrt{[V_i - V_x(x, y_{s2})]^2 + V_y^2(x, y_{s2})}} \quad (42)$$

$$\gamma_{s3} = \frac{|\Delta V_3|}{|U_3|} = \frac{|\Delta V_3|}{\sqrt{[V_{1f} - V_x(x, y_{s3})]^2 + V_y^2(x, y_{s3})}} \quad (43)$$

$$\gamma_{s4} = \frac{|\Delta V_4|}{|U_4|} = \frac{|\Delta V_4|}{\sqrt{[V_{2f} - V_x(x, y_{s4})]^2 + V_y^2(x, y_{s4})}} \quad (44)$$

σ for all frictional surfaces locations (parametric state) is calculated by replacing Eqs. (41) and (44) in Eq. (40), and the shear power losses on surfaces S_1 - S_4 is calculated by Eq. (36).

The velocity discontinuity surface S_1 is determined by:

$$W_{S1} = \frac{1}{\sqrt{3}} \begin{cases} \int_{x_4}^{x_5} \sigma_s \left| (V_y)_{y=y_{s1}} \frac{dy_{S1}}{dx} + (V_x - V_i)_{y=y_{s1}} \right| dx; & x_4 < x_5 \\ \int_{x_5}^{x_4} \sigma_s \left| (V_y)_{y=y_{s1}} \frac{dy_{S1}}{dx} - (V_x + V_{ii})_{y=y_{s1}} \right| dx; & x_4 > x_5 \end{cases} \quad (45)$$

And the velocity discontinuity surface S_2 is determined by:

$$W_{S2} = \frac{1}{\sqrt{3}} \begin{cases} \int_{x_3}^{x_4} \sigma_c \left| (V_y)_{y=y_{s2}} \frac{dy_{S2}}{dz} + (V_x - V_{2i})_{y=y_{s2}} \right| dx; & x_3 < x_4 \\ \int_{x_4}^{x_3} \sigma_c \left| (V_y)_{y=y_{s2}} \frac{dy_{S2}}{dx} - (V_x + V_{2i})_{y=y_{s2}} \right| dx; & x_3 > x_4 \end{cases} \quad (46)$$

The velocity discontinuity surface S_3 is determined by:

$$W_{S3} = \frac{1}{\sqrt{3}} \int_{x_0}^{x_1} \sigma_s \left| (V_y)_{y=y_{s3}} \frac{dy_{S3}}{dx} - (V_x + V_f)_{y=y_{s3}} \right| dx \quad (47)$$

And for surface S_4

$$W_{S4} = \frac{1}{\sqrt{3}} \int_{x_1}^{x_2} \sigma_c \left| (V_y)_{y=y_{s4}} \frac{dy_{S4}}{dx} - (V_x + V_f)_{y=y_{s4}} \right| dx \quad (48)$$

And the total shear power losses is:

$$W_S = W_{S1} + W_{S2} + W_{S3} + W_{S4} \quad (49)$$

2.7.3. The friction power losses

The general equation for the friction power losses for a surface with a constant friction factor m is:

$$W_f = \frac{m}{\sqrt{3}} \int_S \sigma |\Delta V| dS \quad (50)$$

For surface S_5 :

$$|\Delta V_5| = |(V_x)_I|_{y=y_1} \sqrt{1 + y_1'^2} \quad (51)$$

$$dS_5 = \frac{dx}{\cos \alpha}$$

$$\bar{\epsilon} = \int_{y_1} d\epsilon_{eq} = \int_0^{x_5} \frac{d\epsilon_{eq}}{dt} \frac{dt}{dS_5} dS_5 = \int_0^{x_5} \frac{\dot{\epsilon}_{eq}(x, y_1)}{\sqrt{V_x^2(x, y_1) + V_y^2(x, y_1)}} dS_5 \quad (52)$$

Where $\cos \alpha$ is determined from the following equation:

$$\cos \alpha = \frac{x_5}{\sqrt{x_5^2 + (t_{1i} - t_{1f})^2}} \quad (53)$$

For S_6 :

$$|\Delta V_6| = |(V_x)_I - (V_x)_{II}|_{y=y_2} \sqrt{1 + y_2'^2} \quad (54)$$

$$dS_6 = \frac{dx}{\cos \gamma}$$

$$\bar{\varepsilon} = \int_{y_2} d\varepsilon_{\varepsilon q} = \int_{x_1}^{x_4} \frac{d\varepsilon_{\varepsilon q}}{dt} \frac{dt}{dS_6} dS_6 = \int_{x_1}^{x_4} \frac{\dot{\varepsilon}_{\varepsilon q}(x, y_2)}{\sqrt{V_x^2(x, y_2) + V_y^2(x, y_2)}} dS_6 \quad (55)$$

Where $\cos \gamma$ is determined from the following equation:

$$\cos \gamma = \frac{x_4 - x_1}{\sqrt{(x_4 - x_1)^2 + (t_{2i} - t_{2f})^2}} \quad (56)$$

σ for all frictional surfaces locations (parametric state) is calculated by replacing Eqs. (52) and (55) in Eq. (26), and the friction power losses on surfaces S_5 and S_6 can be calculated by replacing in Eq. (50):

$$\dot{W}_{s5} = \frac{m_1}{\sqrt{3} \cos \alpha} \int_0^{x_5} \sigma_s y_1 |(V_x)_I|_{y=y_1} \sqrt{1 + y_1'^2} dx \quad (57)$$

$$\dot{W}_{s6} = \frac{m_2}{\sqrt{3} \cos \gamma} \int_{x_1}^{x_4} \sigma_c y_2 |(V_x)_I - (V_x)_{II}|_{y=y_2} \sqrt{1 + y_2'^2} dx \quad (58)$$

Where m_1 and m_2 are the mean friction factors between the outer layer and the die and between two materials, respectively. The total Shear power loss is determined by:

$$\dot{W}_f = \dot{W}_{s5} + \dot{W}_{s6} \quad (59)$$

2.8. Drawing force

The externally supplied power of deformation is:

$$J^* = \dot{W}_i + \dot{W}_s + \dot{W}_f \quad (60)$$

And the required drawing force for the process is:

$$F_d = \frac{J^*}{V_f} \quad (61)$$

3. Results and Discussion

A MATLAB program has been utilized for the previously derived equations and has been used to study the plastic deformation for different die shapes and friction conditions. The input information, including the initial and final thickness of the sheet, the friction factor, the material type and the die geometry, is imported to MATLAB. The velocity field, strain rate, powers and drawing force are calculated after the calculation of the stream functions.

Table 1 shows the mechanical properties of the sheets.

Table 1 The mechanical properties of the sheets [7]. Material type	Density (kgm ⁻³)	Modulus of elasticity (GPa)	Poisson's ratio	Yield stress (MPa)	The effective stress strain relation (MPa)
Aluminium	0.271	69	0.33	34.5	210 $\varepsilon^{0.3}$
Copper	0.896	117	0.34	70	416 $\varepsilon^{0.2}$

Figure 2 shows the dimension and type of multilayer sheet metal layers in FE model. Figure 3 illustrates the steps of the deformation of multilayer sheet metal simulated by ABAQUS software. The outer layer becomes separate from the inner layer and inclines to the die after the simulation, in the inlet of the die

(Fig. 3b). The Simulation is repeated when the frictionless barrier is on that way (Fig. 3c). Comparing the results obtained from these two conditions (Table 2) shows that the drawing forces are very close. Therefore, the second condition (with barrier) is used since the outer layer of the sheet in the inlet of the zone should be horizontal and the analytical solution is simpler.

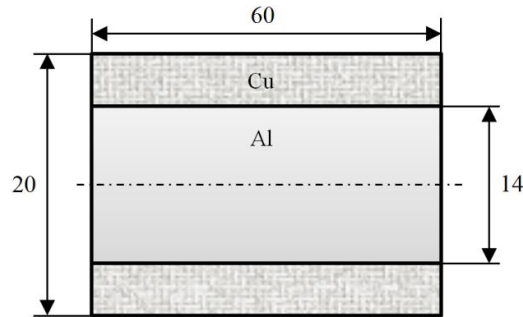
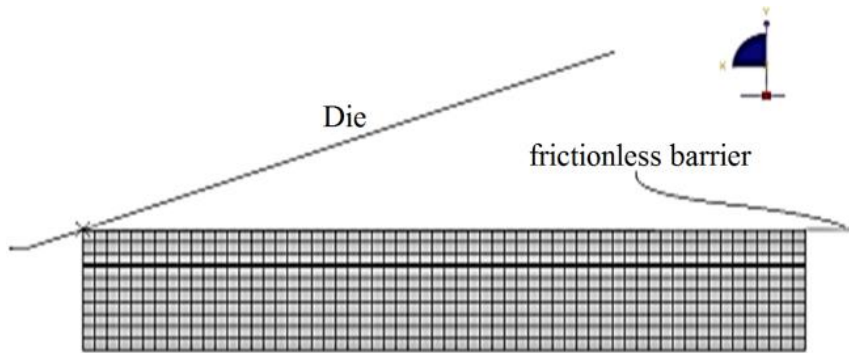
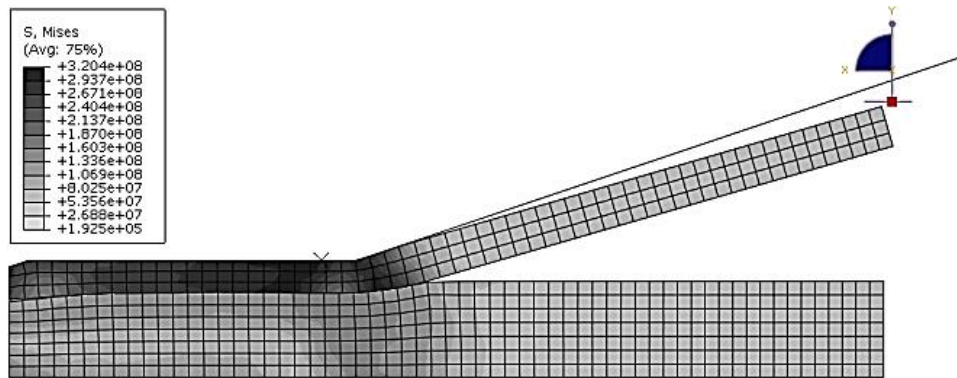


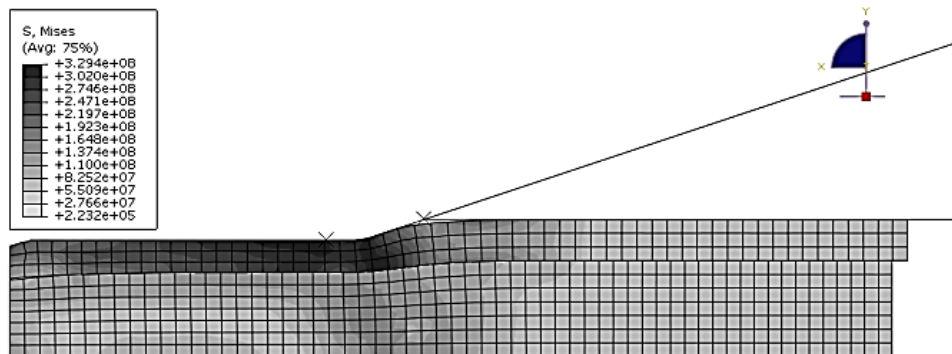
Fig. 2 Configuration of multilayer sheet metal before the process (dimensions are in mm).



a. The schematic of the sheet, in ABAQUS software before the process.



b. Bowed outer layer of the sheet in the input deformation to the die after the process.



c. The effect of the frictionless barrier on the prevention of the movement of the outer layer sheet to the die in the input deformation.

Fig. 3 The schematic of the sheet.

In Table 2, the drawing force in two conditions, with and without barrier, for $m=0.15$ are compared. As shown in this table, the drawing forces in two conditions are the same. Therefore, the second condition (without barrier) is used for comparison with the analytical results.

Table 2. Compares the drawing force in both the presence and absence of the frictionless barrier.

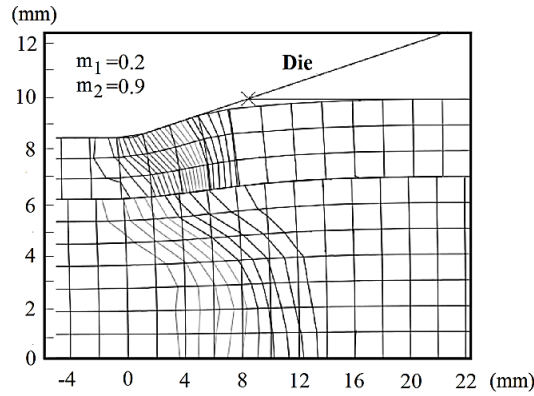
Reduction in thickness %	Drawing force (Newton)		Difference %
	Without barrier	With barrier	
10	693.6	685.5	1.1
20	1285.4	1276.2	0.07
30	1788.5	1772.6	0.08
40	2420.7	2410.5	0.04

Table 3, presents the optimum semi die angle, α , x_1 , x_2 , x_3 , x_4 and t_{1f} . The present drawing force and t_{1f} are compared with the results obtained from the FE model. This comparison has been done for $m_1=0.2$, $m_2=0.9$, $v_f=1$ (mm/s), $t_{1i}=3$, $t_{2i}=7$ (mm) and different reductions. As shown in this table, the inlet and outlet shear boundaries of the deformation zone are being inclined to the inlet zone of the die by increasing the reduction of the thickness. According to table 3, both the thickness of the outlet sheets and the calculated forces are close to FE result.

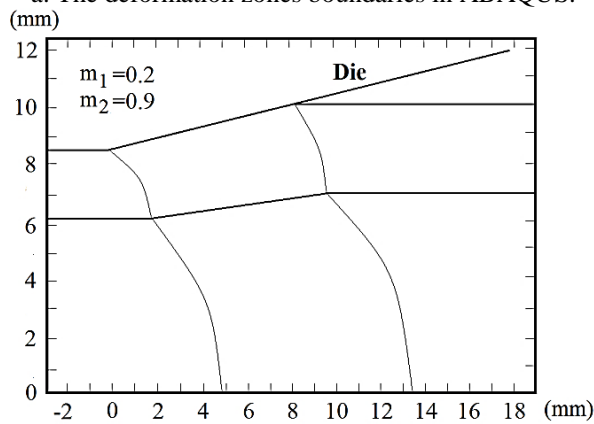
Table 3 Comparison of the presented solution and FEM by considering different reductions.

Reduction	The calculated parameters	presented solution	FEM	Difference %
10	F(N)	734.5	693.6	5.6
	α (deg)	12	-	-
	x_1 (mm)	1.23	-	-
	x_2 (mm)	2.86	-	-
	x_3 (mm)	12.07	-	-
	x_4 (mm)	8.54	-	-
	t_{1f} (mm)	2.72	2.69	1.10
20	F(N)	1341.2	1285.4	4.2
	α (deg)	15	-	-
	x_1 (mm)	2.76	-	-
	x_2 (mm)	5.92	-	-
	x_3 (mm)	14.38	-	-
	x_4 (mm)	10.90	-	-
	t_{1f} (mm)	2.41	2.39	0.83
30	F(N)	1850.6	1788.5	3.5
	α (deg)	21	-	-
	x_1 (mm)	2.97	-	-
	x_2 (mm)	6.37	-	-
	x_3 (mm)	16.84	-	-
	x_4 (mm)	11.52	-	-
	t_{1f} (mm)	2.18	2.16	0.92

In Fig. 4 the boundaries of the deformation zones in the presented analysis and FE model are compared for the specified friction factor and 15% reduction in thickness. It is observed that the deformation zones boundaries of the presented solution is adapted with FE model. This is because the work hardening and the flexible boundaries have been considered.



a. The deformation zones boundaries in ABAQUS.



b. The deformation zones boundaries in the presented solution.

Fig. 4 Comparison of the deformation zones boundaries in the presented solution and FEM.

Figure 5 shows the comparison of the results of the analytical analysis and those of FE for $m_1=0.1$ and $m_2=0.8$ and the effect of the reduction in the area on the optimum semi die angle. As shown in this figure, the required drawing force and the optimum semi die angle are increased by increasing the reduction in the area. Moreover, it is observed that if the semi die angle is larger than the optimum semi die angle, the drawing force will increase. It seems that increase in the reduction of the thickness leads to turbulence in the shear boundaries, and therefore the shear power losses in the inlet and the outlet shear boundaries will increase. Therefore, the drawing force is raised by increasing the shear power losses. In Fig. 7, the results obtained from the present study and FE model are compared. As shown in this figure, the results show good congruence between the analytical solution and FE simulation.

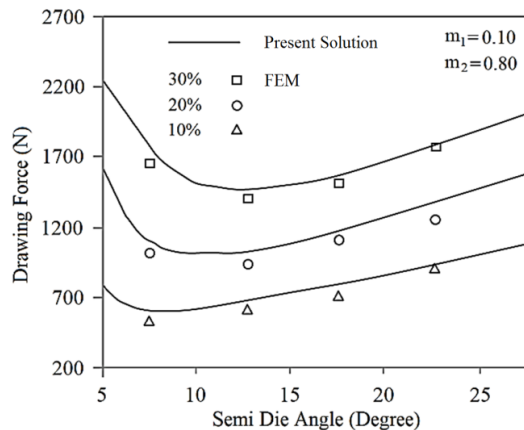


Fig. 5 Comparison of the results of the presented solution and FE for $m_1=0.1$ and $m_2=0.8$ and the effect of the reduction in the area on the optimum semi die angle.

Figure 6 shows drawing force versus semi die angle for different friction factors. This figure also indicates that the optimum semi die angle is improved by increasing the friction factor.

Figure 7 also shows the effect of the work hardening exponent on the required drawing force. It is observed that the required drawing force decreases by increasing the work hardening exponent.

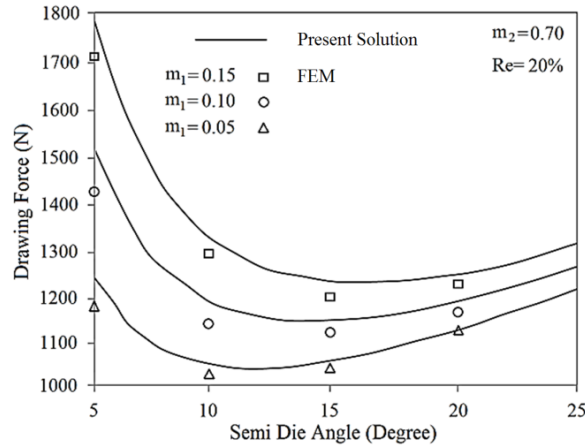


Fig. 6 The effect of changing m_1 on the optimum semi die angle and the comparison of the results of the presented solution and FE for $Re=20\%$.

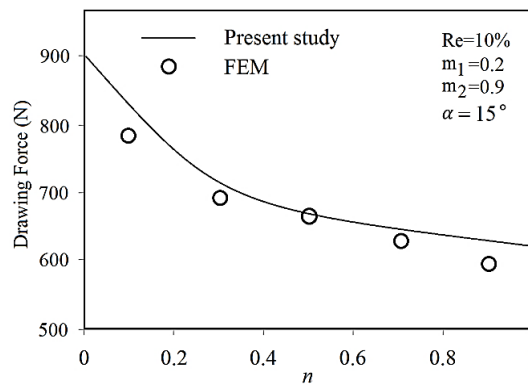


Fig. 7 The effect of changing the work hardening exponent on the required drawing force.

4. Conclusions

In this paper, the drawing process of multilayer sheet metal through a wedge-shaped die has been analyzed using the stream function and the upper bound method. The following results are obtained:

- 1- Considering the flexible boundary and the work hardening leads to good congruence between the results of the presented model and FE.
- 2- It is observed that the required drawing force and the optimum semi die angle will increase by increasing the reduction in thickness and raising the friction factor.
- 3- The results show that the inlet and the outlet shear boundaries of the deformation zone are being inclined to the inlet zone of the die by improving the reduction in thickness.
- 4- The required drawing force decreases by increasing the work hardening exponent.

5. Nomenclature

Strength factor
 Gradient function of horizontal velocity distribution
 The externally supplied power of deformation
 Friction factor between the die and the outer layer
 Friction factor between the inner and outer layers
 Volume flow rate at any cross-section
 The thickness of sheets at the inlet and outlet of the die

A
 C
 J^*
 m_1
 m_2
 Q
 t_i, t_f

Work hardening exponent	n
Velocity discontinuity surfaces	$S_1 - S_4$
Friction surfaces	$S_5 - S_6$
Velocity of the sheet at the inlet and outlet of the die	V_i, V_f
Velocity in the horizontal and vertical direction	V_x, V_y
Difference of tangential velocity at velocity discontinuity surfaces	$\Delta v_1 - \Delta v_4$
Difference of friction velocity	$\Delta v_5 - \Delta v_6$
Friction power losses along the wall, internal power of deformation and shear power losses along the surface of velocity discontinuity, respectively	W_f, W_i, W_s
Boundary function along the surface of the die	y_1
Boundary function along interface between sheets	y_2
Boundary function along deformation zones boundaries	$y_{s1} - y_{s4}$

Greek letters

Semi die angle	α
Angle along the middle surface of both metals	γ
Engineering shear strain	γ_s
Strain rate of the material	$\dot{\epsilon}$
Flow stress of the inner layer	σ_c
Flow stress of the outer layer	σ_s
Effective strain along the stream line	$\bar{\epsilon}$
Stream function	ϕ
Derivative of () with respect to x	$()'$

Subscripts

After drawing (or at the exit of the die)	f
Before drawing (or at the entrance of the die)	i
Outer layer	1
Inner layer	2

6. References

- [1] R. R. Arnold, P. W. Whitton, Stress and Deformation Studies for Sandwich Rolling Hard Metals, *Proceedings of the Institution of Mechanical Engineers* 173 (1959) 241-256.
- [2] A. G. Atkins, A. S. Weinstein, The Deformation of Sandwich Materials, *International Journal of Mechanical Sciences* 12 (1970) 641-657.
- [3] K. Osakada, Y. Niimi, A Study on Radial Flow Field for Extrusion Through Conical Dies, *International Journal of Mechanical Sciences* 17(1975) 241-254.
- [4] B. Avitzur, Analysis of Wire Drawing and Extrusion Through Dies of Large Cone Angle, *Journal of Engineering for Industry, Trans. ASME* 86 (1964) 305-316.
- [5] D. Durban, Drawing and Extrusion of Composite Sheets, Wires and Tubes, *International Journal of Solids and Structures* 20 (1984) 649-666.
- [6] H. Tokuno, Analysis of Deformation in Extrusion of Composite Rods, *Journal of Materials Processing Technology*, 26 (1991) 323-335.
- [7] A. K. Taheri, S. A. Majlessi, An Investigation into the Production of Bi- and Tri-Layered Strip by Drawing Through Wedge-Shaped Dies, *Journal of Materials Engineering and Performance* 1 (1992) 285-291.
- [8] A. Karimi Taheri, Analytical Study of Drawing of Non-Bonded Trimetallic Strips, *International Journal of Machine Tools and Manufacture* 33 (1993) 71-88.
- [9] Chitkara N.R., Aleem A., Extrusion of axisymmetric bi-metallic tubes: some experiments using hollow billet and the application of a generalized slab method of analysis, *International Journal of Mechanical Sciences* 43(2001) 2857-2882.

- [10] Chitkara N.R., Aleem A., Extrusion of axisymmetric bimetallic tubes from solid circular billets: application of a generalized upper bound analysis and some experiments, *International Journal of Mechanical Sciences* 43 (2001) 2833–2856.
- [11] Hwang Y.M., Hwang T.F., An investigation into the plastic deformation behaviour within a conical die during composite rod extrusion, *Journal of Materials Processing Technology* 121 (2002) 226-233.
- [12] E. M. Rubio, M. A. S. Perez, A. S. Lobera, Mechanical solutions for drawing processes under plane strain conditions by the upper bound method, *Journal of Materials Processing Technology* 143-144 (2003) 539-545.
- [13] Kazanowski P., Epler M.E., Misiolek W.Z., Bimetal rod extrusion-process and product optimization, *Materials Science and Engineering* 369 (2004) 170–180.
- [14] Nowotynska I., Smykla A., Influence of die geometric parameters on plastic flow of layer composites during extrusion process, *Journal of Materials Processing Technology* 209 (2009) 1943-1949.
- [15] Khosravifard A., Ebrahimi R., Investigation of parameters affecting interface strength in Al/Cu clad bimetal rod extrusion process, *Materials and Design* 31 (2010) 493-499.
- [16] M. Malaki, H. R. Roohani, Investigation of the Bimetal Clad Drawing by Upper Bound Method, *Journal of Materials Engineering and Performance* 22 (2013) 943-951.
- [17] H. Haghighat, P. Amjadian, A Generalized Upper Bound Solution for Extrusion of Bi-Metallic Rectangular Cross-Section Bars Through Dies of Any Shape, *Journal of Theoretical and Applied Mechanics* 51 (2013) 105-116.
- [18] H. Haghighat, H. Shayesteh, Upper Bound Analysis for Hybrid Sheet Metals Extrusion Process Through Curved Dies, *Transactions of Nonferrous Metals Society of China* 24 (2014) 3285-3292.
- [19] A. Panteghini, An analytical solution for the estimation of the drawing force in three dimensional plate drawing processes, *International Journal of Mechanical Sciences* 84 (2014) 147-157.

شکل دهی ورق ساندویچی متقارن با فرآیند کشش: تحلیل و شبیه سازی

یوسف ملاپور^{1*}، داود افشاری²، حشمت اله حقیقت³
¹گروه مهندسی مکانیک، دانشگاه زنجان، زنجان، ایران.
²دانشکده مهندسی مکانیک، دانشگاه رازی، کرمانشاه، ایران.

چکیده: در این مقاله، فرآیند کشش ورق های ساندویچی متقارن با قالب گوه ای شکل، با استفاده از تابع جریان و به روش کرانه بالایی تحلیل شده است. ورق ساندویچی دارای سه لایه فلز بوده که ضخامت و جنس لایه های خارجی یکسان و متفاوت با لایه داخلی می باشند. در مقاله حاضر یک مدل تغییر شکل ارائه شده که در آن مرزهای برشی ورودی و خروجی نواحی تغییر شکل، انعطاف پذیر بوده و اثر کارسختی مواد لایه های تشکیل دهنده ورق، لحاظ شده اند. بر اساس تابع جریان پیشنهادی، میدان سرعت، نرخ کرنش ها و توان ها محاسبه شده اند. شکل هندسی بهینه نواحی تغییر شکل لایه های داخلی و خارجی و نیروی کشش لازم برای انجام فرآیند، بر اساس شرایط فرآیند محاسبه شده اند. همچنین نتایج تحلیل شامل نیروی کشش و ضخامت لایه ها در خروجی قالب با نتایج به دست آمده از شبیه سازی اجزا محدود مقایسه شده اند. مقایسه نتایج تحلیلی با نتایج به دست آمده از شبیه سازی تطابق مناسبی را نشان داده اند. در پایان نیز تاثیر ثابت اصطکاک و درصد کاهش ضخامت بر نیروی کشش و زاویه ی بهینه ی قالب بررسی شده اند.

واژه های کلیدی: کرانه بالایی، کارسختی، فرآیند کشش ورق، ناحیه تغییر شکل، تابع جریان.